⊙ Scientific Paper

Effects of Welding Parameters on Weld Strength and Acoustic Emission in Friction Welding*

by Sae Kyoo Oh** and Kuo-King Wang***

마찰용접에 있어서 용접강도와 AE에 미치는 용접조건의 영향에 관한 연구

오 세 규 · 쿠오 킹 왕

요 약

경제성과 압접성능의 우수성 때문에 일반 산업기계, 방위산업기계 및 우주항공기계등의 부품생산에 응용되고 있는 마찰 용접에 있어서, 현재 주 관심사 중의 하나는 용접강도에 대한 신뢰성 높은 공정중 비파괴 검출이며 이들의 실용화를 위한 정량적 해석이다. 그러나 이러한 연구는 아직 개발 완성되지 못하고 있다.[1,2]

본 연구에서는, AE 법에 의한 용접강도의 공정중 비파괴적 QC시스템 개발을 최종 목적으로 한 설계자료를 얻기 위하여, 이종강의 봉과 봉, 관과 관의 마찰용접강도와 AE 총누적량에 용접조건이 미치는 영향이 실험적으로 조사 되었고, 회전 속도를 매개 변수로 하여 용접강도와 AE 총 누적량과의 정량관계가 수립되었다.

1. Introduction

In this study, acoustic emission technique is applied to inertia friction welding as a promissingly reliable and repeatable quality monitoring method to examine the effects of main welding parameters (inertia, rotating speed and axial pressure) on the weld strength (tensile strength) and acoustic emission counts in inertia welding of heat resisting low alloy steel bars (AISI 4140) to sulphurized free machining steel bars (AISI 1117, 12L14) and low carbon steel tubes (AISI 1020) to austenite stainless steel tubes (AISI 304).

Finally, the empircal equations are comuted by the regression analysis using the least squares method through several confirmatory trials for the closest similar predicting functions (e.g. first order, quadratic, cubic, power function, etc.) according to the experimental data, and then checked for the adequacy at 95% confidence by error analysis and lack-of-fit test. And the comparison between empirical and calculated equations for relationship between weld strength and total AE counts are made to be utilized for quality control.

Consequently, the objectives of this study are as the following :

* Paper presented at the Spring Annual Convention (Apr. 23, 1982) of the KOSME.
** Member, Professor of National Fisheries Univ. of Busan, Dept. of Mech. Eng.
*** Professor of Cornell University, Sibley School of Mech. and Aerospace Eng.

(1) To examine the effects of welding parameters (inertia, rotating speed, pressure) on the weld strength and total AE counts,

(2) to determine the optimum welding conditions for the joint efficiency more than 100% and

(3) to make the quantitative relationship equations between rotating speed n and weld strength (tensile strength) σ_T or total AE counts N, and then the calculated σ_T-N equation.

2. Experimental Setup and Procedures

Fig. 1 shows the dimensions of welding workpieces and tension test specimens. About eighty work pieces for each welding material were prepared.

The chemical compositions of base metals are shown in Table 1.

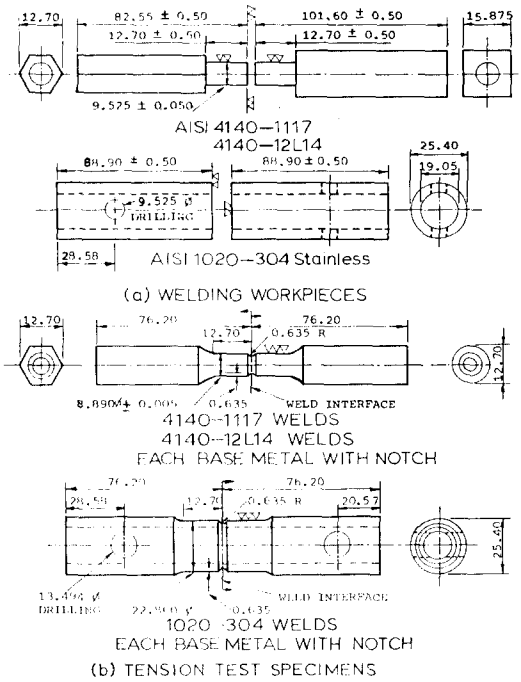

Fig. 1 Welding workpieces and tension test specimens.

Table 1 Chemical compositions and tensile strength.

Materials (AISI)	Chemical composition (wt %)									T.S* σ_T
	C	Mn	P	S	Pb	Cr	Mo	Ni	Si	
4140	0.38	0.75	0.04	—	—	0.80	0.15	—	0.20	113.4
1117	0.17	1.00	0.04	0.08	—	—	—	—	—	72.1
12L14	0.15	0.85	0.04	0.26	0.15	—	—	—	—	66.9
1020	0.20	0.45	0.04	0.05	—	—	—	—	—	62.2
304 S.S.	0.08	2.00	0.04	0.03	—	18.0	—	8.00	0.75	75.5

* Unit; kgf/mm², each specimen with 0.635mm R notch.

For friction welding, an experimental inertia welding machine (automatic controlled inertia welder) was used, which is run by a hydraulic motor and pressed axially by pneumatic power. Table 2 lists the welding conditions.

For tension test of friction welds, the universal testing machine (Instron 1114) was used. The tension loading speed was 2.54 mm/min.

The AE transducer location diagram and the block diagram of electronic components for AE monitoring equipment and welding

Table 2 Welding conditions.

Materials combination (AISI)	Diameter D, mm	Moment of inertia I, kgfm²	Initial rotating speed n, rpm	Axial pressure p, kgf/mm²
Bar-to-bar 4140-1117	9.525	0.236	937-3450	12.7, 19.1, 25.5
Tube-to-tube 1020-304 SS	OD 25.40 ID 19.05	0.472	796-2984	8.2

-parameters measuring apparatus are given in Fig. 2 (a) and (b), respectively. A 22.225 mm diameter acoustic emission piezoelectric transducer (Dunegan/Endevco Model D9203, sensitivity -66 db) was mounted on the jaw 53.85 mm away longitudinally from the welding interface and 40.64 mm away transversely from the centerline of workpiece.

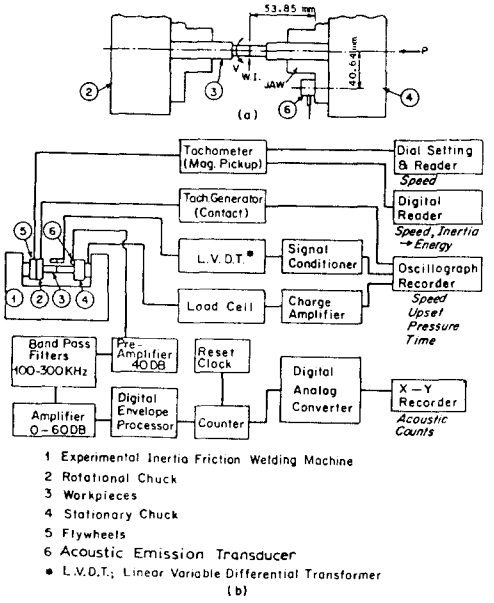

Fig. 2 (a) AE transducer location,
(b) Block diagram of AE monitoring equipment and welding parameters measuring apparatus.

The AE equipment was a standard commercial unit (Dunegan/Endevco Model 3000). For two specimens, under each welding condition, a reset clock was used, while for one, the cumulative total counts were obtained by using 'Memory' set.

For investigating AE results, the count rate was converted to the cumulative total counts as the following by measuring the area of Zone A and B with a planimeter;

(Total Counts)
=2(Area of Zone A+B)
×(X-axis Sweep Time)
×(Full Scale AE Counts/10)
×(1 Pulse Interval),
$[(mm^2)\times(sec/mm)\times(counts/volt)/(mm/volt)\times(1/sec)]$ ·····(1)

The results analyzed by Equation (1) were coincident with the cumulative total counts obtained directly from the digital window by 'Memory' setting.

Also, at the same time, rotational speed, pressure (thrust force) and upset versus time (sec) were recorded with the same X-axis sweep time using a separate oscillographic recorder.

The history of welding parameters and the typical AE measurement in Fig. 3 (a) and (b), respectively. In Fig. 3 (a), under 907.2 kgf (gage pressure 1.0547×10^{-2} kgf/mm^2) setting, the thrust force (kgf) curve reaches the first peak at about 0.2 sec after welding start under the rotating speed (n, rpm) of 1553 rpm in Phase I (friction and heating area) and decreases in Phase II (shearing plastic deformation area) like the torque curve. The total upset (U, mm) curve is constant du-

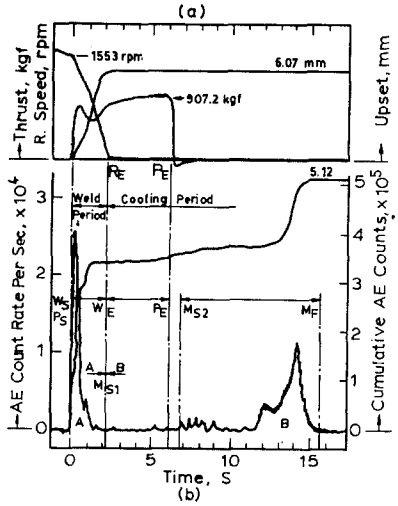

Fig. 3 History of welding parameters and AE measurement in inertia friction welding:
(a) History of welding parameters for 9.525 mmϕ bar-to-bar weld of 4140 to 1117 steels (Inertia: I=0.236 kgfm^2),
(b) AE count rate and cumulative AE counts, (Gain: 75 db).

ring cooling period after speed drops to zero resulting in the welding period end. The moment of inertia was 0.236 kgfm² by setting one flywheel.

In Fig.3 (b), AE count rate and cumulative AE counts curves were given by setting with RATE and MEMORY, respectively on the AE instrumental system. Total counts from the AE count rate curve were calculated by Equation (1) as described above for analyzing AE of Zone A in welding period and Zone B in cooling period.

3. Results and Discussions

3-1. Effect of Rotating Speed

In Fig.4, the experimental results about the effects of rotating speed on the inertia friction weld strength (tensile strength) for 9.525 mmϕ bar-to-bar weld of AISI 4140 to 1117 steels and 25.40 mmϕ tube-to-tube weld of AISI 1020 to 304 stainless steels are shown.

The empirical equations of the friction welded joint strength (tensile strength, σ_T, kgf/mm²) versus rotating speed (n, rpm) computed by the least squares method from the experimental data are as follows;

For 4140-1117 welds,

$$\sigma_T=-9.2195\times10^{-6}n^2+33.582\times10^{-3}n+46.55,$$

($1010\leqq n\leqq 3450$, Eq. adequacy; mean % error 3.29) ·····(2)

For 1020-304 tube welds,

$$\sigma_T=-28.463\times10^{-6}n^2+107.71\times10^{-3}n-30.18,$$

($1261\leqq n\leqq 2569$, Eq. adequacy; mean % error 1.16)·····(3)

For analysis convenience, the σ_T-n curve for 4140—1117 welds is made to be related to the energy versus speed (E—n) curve which was made from the formula[1]

$$E=In^2/1787.3=132.04\times10^{-6}n^2 \cdots\cdots(4)$$

where the rotational moment of inertia I is 0.236 kgfm² in this experiment, as well as related to V_h-n curve of the burn-off rate V_h (mm/sec) versus welding speed n (rpm) for 4140—1117 welds, which was obtained from experimental results and computed to make the empirical equation as follows;

$$V_h=836.91\times10^{-9}n^2-3.5389\times10^{-3}n+5.09,\ (974\leqq n\leqq 3175,\ \text{Eq.}$$

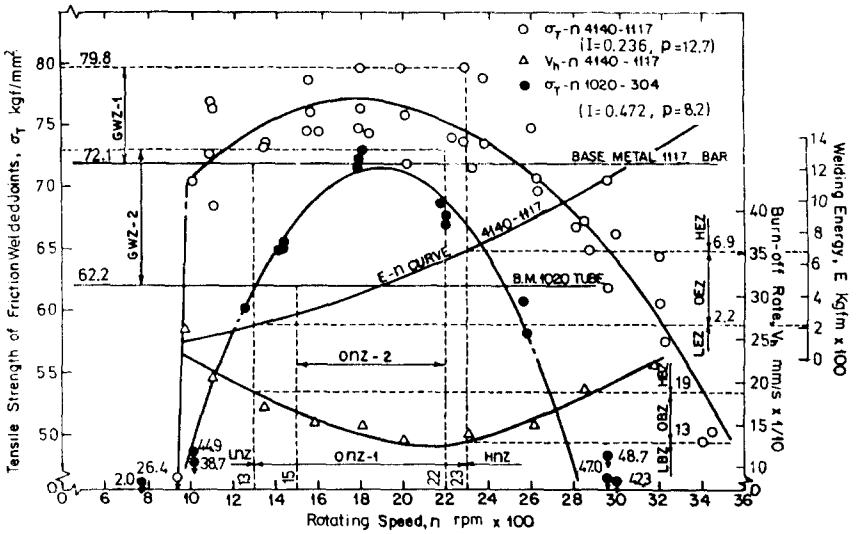

Fig.4 Effect of rotating speed on weld strength for 9.525 mmϕ bar-to-bar welds of 4140 to 1117 steels and 25.4 mmϕ tube-to-tube welds of 1020 to 304 stainless steels.

adequacy; mean % error 4.78) ···(5)

As shown in Fig. 4 and from Equations (2) and (3), it is clear that all these curves have correlation and the weld strength (tensile strength) has dependence upon rotating speed, energy and burn-off rate. To increase welding energy, rotating speed should also be increased. The increase of the rotating speed from low speed to high level speed results in increasing and then decreasing the weld strength, while the burn-off rate, which is obtained from the straight line gradient of axial shortening curve during about 0.2 sec (temperature peak) after weld start in Phase I [3] (Fig. 3), decreases during low level speed and optimum speed zone (OnZ, and then increases during high level speed zone (HnZ). It is reported that welding energy produces the heat necessary for welding and the rate of burn-off, that is the rate of axial compressive deformation, under the steady state in heating phase is related to welding parameters, and the burn-off rate is used practically for quality control in friction welding[4),5),7)-11)].

In this study, therefore, the energy-speed (E-n) and burn-off rate-speed (V_h-n) curves were used only as the intermediaries for analyzing the relationship between weld strength and total AE counts rather than interpreting themselves.

In Fig. 4, for example, in the case of 4140-1117 welds, it is clear that the optimum welding condition for getting to the good weld zone (GWZ-1) with the joint efficiency above 100%, that is more than the tensile strength of base metal 1117, is 1300 through 2300 rpm at optimum rotating speed zone (OnZ-1) between low speed zone (LnZ) and high speed zone (HnZ), and, at the same time, 221.28 through 691.50 kgfm at optimum energy zone (OEZ) and 1.32 mm/s through 1.91 mm/s at optimum burn-off rate zone (OBZ). Thereby, it is found that the optimum (or good) AE zone (GAZ-1) for getting to the good weld zone (GWZ) is 0.54×10^6 through 2.54×10^6 counts at the same optimum zones (OnZ-1, OEZ, OBZ) in Fig. 5 as those in Fig. 4.

In the case of 1020—304 tube welds, the optimum welding conditions for the good

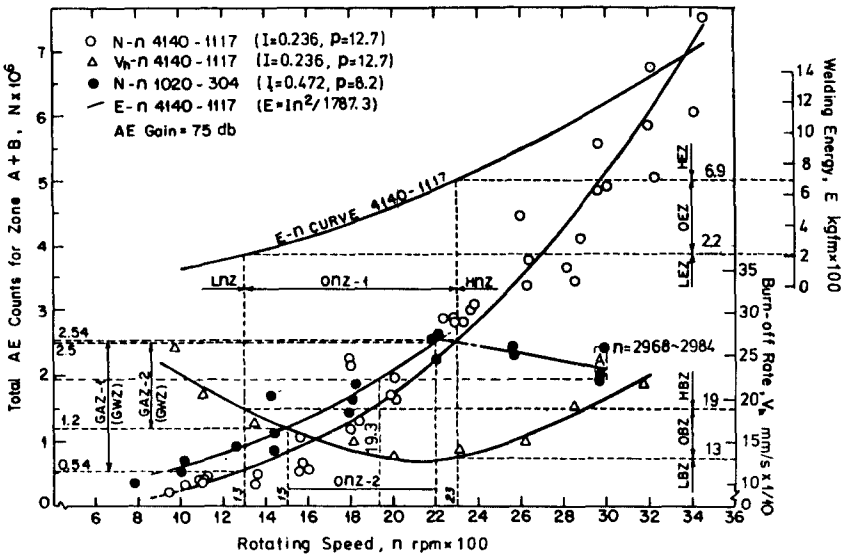

Fig. 5 Effect of rotating speed on total AE counts for 9.525 mmϕ bar-to-bar welds of 4140 to 1117 steels and 25.4 mmϕ tube-to-tube welds of 1020 to 304 stainless steels.

weld zone (GWZ-2) in Fig. 4 is 1500 through 2200 rpm at OnZ-2, where the good AE zone (GAZ-2) is 1.2×10^6 through 2.5×10^6 counts in Fig. 5 for getting to GWZ-2 in Fig. 4.

The above method is the indirect one for monitoring the weld strength by total AE counts through rotating speed plus welding energy and burn-off rate.

It is also known in Fig. 4 that the optimum speed zone (OnZ) should be about 250 rpm away inward from the two intersections of the σ_T-n curve and the tensile strength line of each base metal, because the σ_T-n curve has such a degree of scatter band and the allowance for safety design should be given.

In Fig. 5, the experimental results about the effects of rotating speed on the cumulative total AE counts for 9.525 mmϕ bar-to-bar welds of 4140 to 1117 steels and 25.4 mmϕ (3.175 mm wall) tube-to-tube welds of 1020 to 304 stainless steels are given.

The empirical equations of the total AE counts (N, counts) for Zone A+B versus rotating speed (n, rpm) computed by the least squares method from the experimental data are as follows;

For 4140—1117 welds,

$$N=3.0174\times10^{-3}n^{2.6583},$$

($1010\leqq n\leqq3450$, Eq. adequacy; mean % error 14.50) ……(6)

For 1020—304 tube welds,

$$N=1.9915n^{1.8280},$$

($1019\leqq n\leqq2208$, Eq. adequacy; mean % error 11.28) ……(7)

As shown in Fig. 5 and from Equations (6) and (7), it is clear that those curves have correlation among one another, and the total AE counts have dependence on rotating speed, energy and burn-off rate as described in Fig. 4. In the case of 4140—1117 welding, the increase of the rotating speed from low level to high level speed and consequently the increase of the welding energy results in increasing the total AE counts, while the burn-off rate decreases at low level and optimum speed zones (Lnz, OnZ) and then increases at high level speed zone (HnZ).

In the case of 1020—304 tube welding,

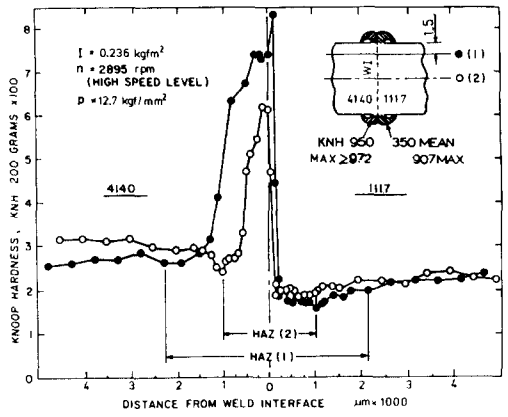

Fig. 6 Hardness distribution of welded joint 4140 to 1117 steel (9.525 mmϕ).

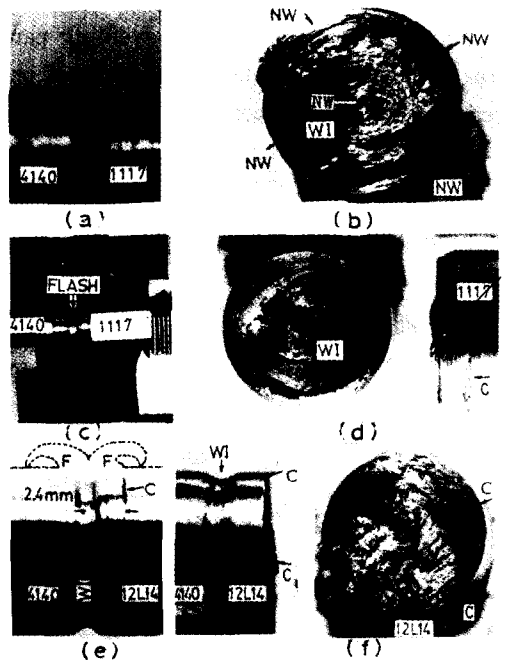

Fig. 7 Typical appearance and fractured surfaces of welded joints:
(a), (b); at lowest speed 937 rpm,
(c), (d); at medium speed 1603 rpm,
(e), (f); at high speed level 2822 rpm.

the increase of speed or energy results in increasing the total AE counts with decrease of burn-off rate initially at low level and optimum speed zones, but, at high level speed zone, decreasing the total AE counts with increase of burn-off rate.

As shown on the σ_T-n curves in Fig. 4, there are the increase, the peak and the decrease zones according to the increase of rotating speed from low to high level. In order to interpret the cause for such fluctuations behavior of weld tensile strength versus total AE counts, some attentive examination and experiments were carried out with the results as shown in Fig. 6 and Fig. 7.

Fig. 6 shows the hardness distributions (Knoop hardness, load 200g) along the centerline and the periphery of 4140 to 1117 joint welded under the welding condition such as I=0.236 kgfm², n=2895 rpm (high level) and p=12.7 kgf/mm². Each distribution diagram has the peak at the adjacent area of weld interface because the weld interface received the heat which, by a report in the case of welding AISI 1020 steel to itself[3], climbs up to about 1300°C only in 0.06 sec at the periphery and then flows toward the center by conduction and becomes almost epualized over the whole interface at the end of 0.2 sec and stays within the range of 1250 to 1350°C after the first 0.2 sec. This high temperature within a few seconds until welding ends (rotating stops) is enough to make the interface hardened by being cooled with the adjacent air and parent metal as a quenching effect, resulting in forming the martensite structure at the welded zone[6].

It was found that such martensite phase transformation from austenite is most significant at the outside flashes with mean KNH 950 on the 4140 side and mean KNH 350 (907 max) on the 1117 side[7].

On each of both sides within 2.29 mm away at the periphery area and 1.02 mm away at the centerline from the interface, there is the weakest area with the lowest hardness, which is lower than that of base metal. This is the boundary area of heat affected zone (HAZ) and base metal. At the HAZ, the hardness at periphery is higher than that at centerline on the 4140 side because the periphery has been more heated and also 4140 steel has more excellent hardenability with the higher carbon contents (0.38%) and with the elements Cr (0.80%) and Mo (0.15%) as martensite formation stabilizers.

On the other hand, the 1117 side periphery hardness is lower than that of the centerline at the HAZ boundary area because the periphery has been more heated but not enough to be hardened because 1117 steel has less hardenability with lower carbon (0.17%) and with no martensite stabilizer, resulting in making it softened rather than hardened[13]. In the case of Fig. 6, the welding was performed at high speed level, so the HAZ is somewhat wide. But it becomes narrower according to the decrease of rotating speed, resulting in the variation of tensile fracture locaiton according to the HAZ boundary movement of 1117 side in the range from about 2 mm area to the weld interface as shown in Fig. 7. These hardness distribution characteristics are well consistent with those of friction welding the Si-Cr alloy (Cr 11%, Si 2%) to high Ni-Cr alloy (Ni 14%, Cr 15%, Si 1.5 %)[8]. Such a severe hardness difference between the interface area and the HAZ boundary causes to make the residual stress, and according as the hot weld zone becomes cooling and shrinks, the HAZ boundary periphery area becomes to get crack initiation and propagation transversely on the periphery surface as shown in Fig. 7.

Fig. 7 shows the typical appearance and tensile fractured surfaces of inertia welds 4140-1117 and 4140-12L14 welded at different rotating speed levels. At the lower speed level, non-welded periphery (NW) occurs by hot tearing of the weld at the periphery of the interface as shown in Fig. 7 (a) and (b), and also the center area of the interface on the fractured surface is not welded due to lack of heat. At the medium (proper) speed level as shown in Fig. 7 (c) and (d), crack occurs initially on the periphery surface of the 1117 side HAZ boundary, that may be the corner between flash and parent material or the corner just before the HAZ boundary surface from the interface. But, as the crack propagates inward of HAZ along the boundary, it stops for the inside is harder than the periphery at the 1117 side HAZ. Instead, the tensile fracture occurs at the weld interface with the notch of 0.635 mm radius. This means that the HAZ strength is just enough not to be fractured at HAZ. The appearance of this tensile fractured surface consists of the ductile fractured outside part and the brittle fractured inside one, that expresses nearly a good weld. At the higher speed level as shown in Fig. 7 (e) and (f), the tensile fracture occurs on the HAZ periphery surface (the flash corner) eventhough it has a notch on the interface, because it had a crack or a few cracks on the HAZ boundary periphery surface occurred during cooling after welding by the thermal stress effect and flash-corner-notch effect before tension test. Such crack phenomena on HAZ boundary surface are especially severer in the case of leaded sulphurized free machining steel 12L14 because of the poor weldability with lead.

Consequently, the variation of the increase and decrease of weld strength with the increase of rotating speed is due to the lack of heat by the lower energy at lower speed level, and on the contrary, it is due to the over-heating by the higher energy at higher speed level resulting in weld defects, that is, crack or residual stress concentration at the flash corner. But, it has also the tendency of the decrease at the higher speed level depending on the difference of cooling rate of materials, resulting in the difference of the martensite start and end temperatures on the CCT curve. The weld of low carbon steel tube 1020 to 304 stainless steel tube has such a tendency, because the latter with very low carbon (C 0.08%) takes longer time (more than 100 sec) to form the martensite at higher speed level, resulting in slower cooling rate and the less martensite formation with the lower AE burst.

3-2. Effect of Welding Pressure

The experimental results of welding axial pressure effect on weld strength and total

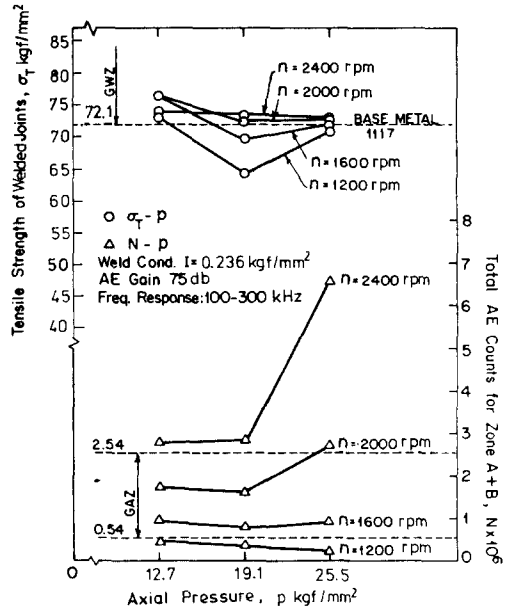

Fig. 8 Effect of pressure on weld strength and total AE counts for 4140-1117 welds (9.525 mmφ).

AE counts in inertia welding of 4140 to 1117 steel bars (9.525mm diameter) welded under various rotating speeds are shown in Fig. 8. It is clear that the higher pressure (25.5 kgf /mm²) at the higher speed level (2400 rpm) causes the higher AE counts but the lower strength (lower joint efficiency). On the contrary, the lower pressure (12.7 kgf/mm²) at the medium speed level (1600, 2000 rpm) in good AE zone (GAZ) causes the medium AE counts but the highest strength (highest joint eficiency). Since welding pressure acts as heating in Phase Ⅰ, as balancing for the effects of thermal softening and strain hardening in Phase Ⅱ, and as forging for bonding in Phase Ⅲ, it is important to determine the proper pressure for good weld as shown in Fig. 8.

Consequently, depending on the pressure effect diagram in Fig. 8, it is found that the optimum welding condition for inertia welding of 4140 to 1117 steel bars (9.525 m m dia.) should be p=12.7 kgf/mm², n= 1600 through 2000 rpm and I=0.236 kgfm² constant. These pressure and speeds are well consistent with the optimum speed zone (OnZ-2) 1300 through 2300 rpm and the good AE zone (GAZ-1) 0.54×10^6 through 2.54×10^6 counts in Fig. 4 and Fig. 5 for obtaining the good welds in GWZ.

3-3. Effect of Inertia

The effects of moment of inertia (I, k gfm²) on the weld strength and total AE counts for inertia welding of 4140 to 1117 steel bars (9.525 mm dia.) welded under the welding conditions of p=12.7 kgf/mm² const., n=1000, 1400, 1800, 2200 and 2600 rpm, I=0.118, 0.236 and 0.472 kgfm² are given in Fig. 9. As known in Fig. 9, it is clear that the optimum weld conditions for good welds are p=12.7 kgf/mm² const., I=0.236 kgfm², n=1400, 1800 and 2200 rpm, which are slso quite consistent with

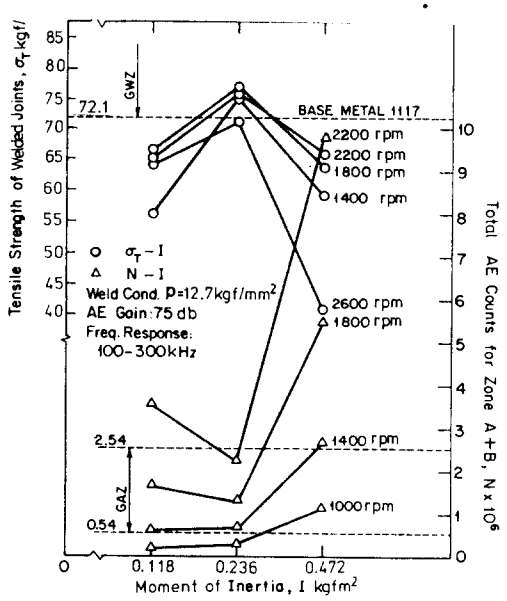

Fig. 9 Effect of inertia on weld strength and total AE counts for 4140-1117 welds (9.525 mmϕ).

the optimum zones of total AE counts and weld strength in Fig. 4 and Fig. 5.

The cause of the variation of both pressure and inertia effects on weld strength and total AE counts can be interpreted by the same method as the speed effects shown in Fig. 4 and Fig. 5, because all these parameters are correlated to the heat generation and forging effect for metallurgical bond.

Since moment of inertia affects the heat generation by energy for bonding metals with rotating speed, it is also necessary to cosnider upon determining the proper inertia by selecting the proper flywheel.

Consequently, it was clarified that weld strength and total AE counts have dependence on rotating speed, pressure and inertia effects.

3-4. Relationship between Weld Strength and Total AE Counts and 95% Confidence Test

From the combination of σ_T-n Equation (2) and N-n Equation (6), the calculated

σ_{Tn}-n Equation for 4140-1117 welds is as follows;

$$\sigma_{Tn}=-731.94\times10^{-6}\ N^{0.75377}+299.23\times10^{-3}\ N^{0.37688}+46.55,\quad (0.283\times10^{6}\leqq N\leqq 7.356\times10^{6})\cdots\cdots(8)$$

where σ_{Tn} is tensile strength σ_T as n was an intermediate variable.

From the combination of σ_T-n Equation (3) and N-n Equation (7), the calculated σ_{Tn}-n equation for 1020-304 welds is as follows:

$$\sigma_{Tn}=-13.368\times10^{-6}N^{1.0971}+73.813\times10^{-3}N^{0.54853}-30.18,\quad (0.895\times10^{6}\leqq N\leqq 2.484\times10^{6}).\ \cdots\cdots(9)$$

For the 95% confidence examination of the empirical N-n Equation (6) with the largest mean % error of 14.5%, the residual sum of squares for the total AE counts was computed as in Table 3, and the ANOVA (analysis of variables) table for testing the lack of fit was calculated as in Table 4. The calculated F-ratio for the lack of fit for the empirical equation is 1.63 which is much smaller than the corresponding value of 3.09 from the F-table at 95% confidence level as shown in Table 3 and Table 4. This analysis suggests that there is no great danger of lack of fit between all the empirical equations and the experimental data in this study.

Tabe 3 Computaion of residual sum of squares and pure error for the total AE counts at the full range of speed on the empirical N-n equation model of 4140-1117 welds.

Trial No.	Total AE count, counts: Expected, N	Observed, N'	Trial No.	Total AE count, counts: Expected, N	Observed, N'
1 a	359550	409000	12	604235	348000
b	359550	386000	13	617436	500000
2 a	900130	682000	14	884923	513000
b	900130	1059000	15	962544	553000
3 a	1310109	2165000	16	1303363	2270000
b	1310109	1196000	17	1383861	1362000
4 a	1759127	1635000	18	1697160	1710000
b	1759127	1973000	19	2302943	2869000
5 a	2461245	2816000	20	2740825	3088000
b	2461245	2912000	21	2578768	2812000
6 a	3571527	3351000	22	2731660	3013000
b	3571527	3755000	23	3462570	4458000
7 a	4890824	5540000	24	4535090	4102000
b	4890824	4827000	25	4435331	3450000
8 a	6038083	5864000	26	4284235	3635000
b	6038083	6730000	27	5063792	4897000
9	282571	320000	28	6141174	5064000
10	349291	407000	29	7356666	7447000
11	364748	419000	30	7121419	6044000

Residual sum of squares $=\sum(N'-N)^2=9.0575\times10^{12}$
Pure error $=1/2\ \sum(N'b-N'a)^2=1.3133\times10^{12}$

Table 4 ANOVA table for testing the lack of fit on the empirical N-n equation model (mean % error: 14.5%) of 4140-1117 welds, at full range of speed.

Source	Sum of squares	Degree of freedom	Mean square	F-ratio
Residual	9.0575×10^{12}	37		
Pure error	1.3133×10^{12}	8	1.6416×10^{11}	
Lack of fit	7.7442×10^{12}	29	2.6704×10^{11}	1.63
Remarks	From F-table: $F_{30,8,0.05}=3.08$, $F_{24,8,0.05}=3.12$, then, $F_{29,8,0.05}=3.09$.			

4. Conclusions

The results of the study[9] on Effects of Welding Parameters on Weld Strength and Acoustic Emission (at Zone $A+B$) in Inertia Friction Welding are as the following:

(1) The optimum range of welding conditions for welding the medium carbon low alloy steels to the sulphurized free machining steels and the mild steels to the stainless steels (tubes) could be determined by the examination of the parameters effects for good weld strength with the joint efficiency more than 100 %, using AE techniques, avoiding the possible weld defects.

(2) It was found that the weld strength (tensile strength) and total AE counts have an intimate dependence quantitatively on the welding parameters, and then their relationship equations can be derived by using one of the parameters as an intermediate variable.

(3) The calculated equations for the relationship between the weld strength (tensile

strength) σ_T and the total AE counts N at Zone $A+B$ in inertia friction welding of AISI 4140 to 1117 (9.525 mmϕ bars) steels and AISI 1020 to 304 (25.4 mmϕ, 3.175 mm wall tubes) stainless steels are as follows, respectively, calculated from the empirical σ_T-n and N-n empirical equations computed by the regression analysis using the least squares method;

$$\sigma_{Tn} = -731.94\times10^{-6}N^{0.75877} + 299.23\times10^{-3}N^{0.37688} + 46.55,$$

$$\sigma_{Tn} = -13.368\times10^{-6}N^{1.0971} + 73.813\times10^{-3}N^{0.54856} - 30.18.$$

It was confirmed by error analysis and lack-of-fit test that all equations have a high reliability at the 95% confidence level.

(4) It was also found that the welding energy or the burn-off rate have a great deal of effects quantitatively upon the total AE counts as well as the weld strength, so that it will be possible to be used as a parameter for monitoring or controlling the weld strength using AE techniques.

(5) It was verified by the examinations of hardness distribution and typical appearance or tensile fractured surfaces that the variations (or droppings) of the weld strength and the total AE counts curves should be, at low speed or high speed level, caused by the weld defects at the weld interface periphery or the HAZ boundary surface area, where the tensile fracture occurred on the base metal side with lower tensile strength, initiating from the crack on the HAZ surface of the specimen with the half circle notch of 0.635 mmR on the interface periphery.

Acknowledgement

The experiments and analyses were carried out at Cornell University, New York, U.S.A., to which lot of thanks are sincerely sent for its providing such useful research facilities. Thanks are also extended to Mr. G. R. Reif of Sandia National Laboratories for his providing the Acoustic Emission Instrument from the SNL.

References

(1) A.W.S., "Welding Handbook", Volume 3, Seventh Edition, Chpt.7, Friction Welding, 1980, p.239—261.

(2) Wang, K. K., Ahmed, S., "Ultrasonic Detection of weld strength for Dissimilar Metal Friction Welds," Proc. of the 4th North American Metalworking Research Conf., 1976, p.384—389.

(3) Wang, K.K., Nagapan, P., "Transient Temperature Distribution in Inertia Welding of Steels," AWS Welding Research Supplement, Sep., 1970, p.419—426.

(4) Fukushima, S., Hasui, A., "Relation between Rate of Burn-off and Welding Conditions in Continuous Drive Friction Welding," Trans. of National Research Inst. for Metals (Japan), Vol.15, No.15, 1973, p.257—266.

(5) Ellis, C.R. G., Nicholas, E.D., "A Quality Monitor for Friction Welding," Proc. of the 3rd Int. Conf. 'Advances in Welding Processes' Horrogate 7-9, May, 1974. The Welding Institute, Paper No.39, p.14—20.

(6) Wang, K.K., Oh, S.K. and Reif, G.R., "In-Process Quality Detection of Friction Welds Using Acoustic Emission Techniques", Proceeding of the 63rd Annual AWS Convention, Technical Session 5-A, in Kansas City, USA, April 27, 1982. WELDING JOURNAL of AWS, Vol.61, No.9, Sept. 1982, p.312—316.

(7) Oh, S. K., A. Hasui, T. Kunio, K. K. Wang, "Effects of Initial Energy on Acoustic Emission Relating to Weld Strength in Friction Welding", Trans. JWS, 13—2, Oct. 1982, p.15—26. Proc. of 4th Int. Sym. JWS, 4JWS-V-8 (Nov. 24—26, 1982), p.713—718.

(8) Oh, S.K., "Study on Friction Welding of Valve Materials···On Improving the Friction Weld Quality···", J. KSME, Vol.14, No.3, 1974, p.221—232.

(9) Oh, S.K., Paper Extracted from Chap. 2 (p.162—204) in Part Ⅱ of "Studies on Strength Analysis of Friction Welded Joints and In-Process Monitoring of the Welding Using Acoustic Emission Techiques," Ph. D. Thesis, Keio University, Japan, 1982.